Diffraction at HERA

Pierre Van Mechelen[1]
(on behalf of the H1 and ZEUS collaborations)
University of Antwerpen (UIA), Belgium [2]

Recent experimental results on the inclusive diffractive cross section at low Q^2 and on jet production in diffractive deep inelastic scattering, obtained by the H1 and ZEUS experiments at HERA, are presented. Various theoretical models for diffractive ep scattering are discussed and confronted with the experimental data.

1 Introduction

It is well known that soft hadron-hadron scattering can be described by Regge phenomenology, which models the total, elastic and single and double diffractive dissociation cross sections in terms of reggeon and pomeron exchange [1]. At high energies, it is the pomeron exchange mechanism that dominates the total cross section [2]. However, until recently, our understanding of the pomeron in terms of Quantum Chromodynamics (QCD) [3] remained fragmentary, at best.

The observation of events with a large rapidity gap in the hadronic final state at HERA [4], which are attributed to diffractive dissociation of (virtual) photons, led to a renewed interest in the study of the underlying dynamics of diffraction. In deep inelastic ep scattering, the long hadronic lifetime of the photon at small Bjorken-x and its variable virtuality Q^2 allow to make the link with diffractive dissociation in hadron-hadron scattering, while the presence of one or more hard scales enables perturbative calculations in QCD.

In the framework of QCD, it is tempting to attribute a partonic structure to the pomeron [5]; an approach which proves to be very successful in describing various aspects of diffractive virtual photon dissociation at HERA. QCD calculations indicate, however, that the pomeron does not exhibit a universal behaviour over the full kinematic range. Indeed, experimental observations of a transition do exist when going from the soft to the hard scattering regime, changing the effective intercept of the pomeron trajectory from 1.08 in the soft limit to 1.2 in harder interactions. Similarly, the application of pomeron parton densities observed at HERA to higher energy $p\overline{p}$ collisions at TEVATRON is not straightforward.

Early experimental measurements at HERA of the inclusive diffractive cross section in deep inelastic scattering [6–9] led to the conclusion that a partonic pomeron would be dominated by hard gluons. This has been qualitatively confirmed by several studies of the properties of the hadronic final state of diffractive virtual photon dissociation [10], which are all in agreement with a substantial contribution from the fragmentation of

[1] Postdoctoral fellow of the Fund for Scientific Research - Flanders (Belgium)
[2] *E-mail address: Pierre.VanMechelen@ua.ac.be*

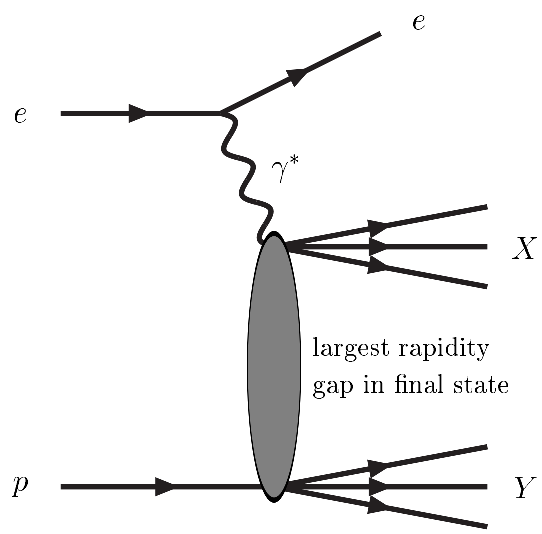

Fig. 1: Illustration of the generic diffractive process $ep \to eXY$.

a colour octet-octet partonic final state, leading to higher particle multiplicities, lower thrust values and a final state that is not strictly aligned with the γ^* axis in the rest frame of the photon dissociation system.

This article presents some recent experimental measurements of the diffractive cross section in an intermediate Q^2 range, thus enabling the study of the transition region between diffractive photoproduction and deep inelastic scattering. A complementary analysis of final states containing two or more jets provides a way to study the gluon content of the pomeron. Moreover, jets with large transverse energy E_T provide an additional hard scale for perturbative QCD calculations.

Following this introduction, Sec. 2 gives a short reminder of the kinematics of diffractive deep inelastic scattering. Section 3 discusses the theoretical models that are used for comparison with the experimental results, Sec. 4 presents the preliminary results, obtained by the H1 and ZEUS collaborations, on the inclusive diffraction cross section at low Q^2 and dijet and 3-jet production in diffractive deep inelastic scattering and, to conclude, a summary is given in Sec. 5.

2 Kinematics of diffractive *ep* scattering

The generic diffractive process $ep \to eXY$ is illustrated in Fig. 1. A photon with virtuality $Q^2 = -q^2$ interacts with the proton to produce the two final state systems X and Y, which are separated by a large rapidity gap if their invariant masses are small.

Cross sections can be expressed in terms of Q^2 and the invariant masses of the $\gamma^* p$ system (W), and the X and Y systems (M_X and M_Y, resp.). In addition, the following variables are usually introduced:

$$x_{I\!P} = \frac{q \cdot (p - p_Y)}{q \cdot p} \approx \frac{Q^2 + M_X^2}{Q^2 + W^2}, \tag{1}$$

$$\beta = \frac{Q^2}{2q \cdot (p - p_Y)} \approx \frac{Q^2}{Q^2 + M_X^2}. \tag{2}$$

In the proton infinite momentum frame, $x_{I\!P}$ is the fraction of the beam proton momentum transferred to X, while β represents the fraction of the exchanged momentum carried by the struck quark. The squared four-momentum transferred at the proton vertex (t) has been neglected in the above equations.

3 Theoretical models

Theoretical models for diffractive deep inelastic scattering range from purely phenomenological parameterizations with a large number of degrees of freedom to full perturbative QCD calculations. The following briefly discusses those models that are used here for comparisons to experimental data.

The partonic pomeron

When measuring the diffractive cross section in deep inelastic scattering at HERA, it was soon recognized that the $x_{I\!P}$ dependence can be modeled exploiting Regge factorization [11], provided that a sub-leading exchange is allowed to contribute at high values of $x_{I\!P}$. In this model, the diffractive cross section factorizes into pomeron and reggeon flux factors, depending on $x_{I\!P}$ only, and into pomeron and reggeon structure functions, depending on β and Q^2. The flux factors describe the long distance physics at the proton vertex and can be parameterized using Regge theory, while the structure functions are free parameters containing the short distance physics at the photon vertex.

Recently, QCD factorization has been proven to hold for the leading twist component of diffractive deep inelastic scattering [12], allowing to further interpret the structure functions in terms of quarks and gluons by applying a QCD motivated model for their β and Q^2 dependence [5,13]. Parton density functions for the pomeron have thus been extracted from the measured cross section, assuming the pion structure function for the sub-leading reggeon exchange and the next-to-leading order DGLAP equations [14] for the evolution in Q^2.

The outcome of these combined Regge-QCD fits is a value of around 1.2 for the pomeron intercept $\alpha_{I\!P}(0)$ and a pomeron structure function that is dominated by gluons carrying large fractional momenta [7].

Soft colour interaction model

A model that does not use the notion of a pomeron at all, is the soft colour interaction model [15]. Instead, the standard matrix element and parton shower description of deep inelastic scattering is used, which, at low Bjorken-x, is dominated by boson-gluon fusion. In addition, non-perturbative interactions affect the final colour connections between partons, while leaving the parton momenta unchanged. This may result in regions void of colour flow, thus creating a large rapidity gap in the final state. The probability for such a soft colour interaction has to be fixed by the experimental data.

Recently, an improved version of this model has become available, which is based on a generalised area law and which favours soft colour interactions that shorten the colour strings between partons [16].

Saturation model

In this and the subsequent models, the virtual photon is considered to fluctuate in partonic configurations, like e.g. $q\overline{q}$ or $q\overline{q}g$. In the proton rest frame and at low Bjorken-x, this happens long before the actual interaction with the proton. Both states, $q\overline{q}$ and $q\overline{q}g$, can be described by dipole wave-functions. These wave-functions are responsible for the basic shape of the β dependence of the diffractive structure function. Three contributions have been introduced [17], two of which are related to the production of $q\overline{q}$ pairs by longitudinally or transversely polarised photons, while a third contribution takes the radiation of an additional gluon into account for the case of a transversely polarised photon:

$$F_{q\overline{q}}^{L} \sim \frac{Q_0^2}{Q^2} \ln\left(\frac{Q^2}{4Q_0^2\beta}\right) \beta^3(1-2\beta)^2, \tag{3}$$

$$F_{q\overline{q}}^{T} \sim \beta(1-\beta), \tag{4}$$

$$F_{q\overline{q}g}^{T} \sim \alpha_S \ln\left(\frac{Q^2}{Q_0^2}\right)(1-\beta)^3. \tag{5}$$

From these formulae, it is clear that $q\overline{q}g$ states are expected to populate the low β (i.e. high mass) region, while $q\overline{q}$ states dominate at intermediate and high values of β. Note that the longitudinal $q\overline{q}$ contribution is of higher twist nature and that the longitudinal cross section is expected to dominate over the transverse cross section at high β.

The subsequent models differ in the way they treat the actual dipole-proton interaction.

An attempt to describe the saturation of the inclusive cross section at low Q^2 and low x leads to the following parameterization of the dipole-proton cross section [18]:

$$\hat{\sigma}(x, r^2) = \sigma_0 \left[1 - \exp\left(-\frac{r^2}{4R_0^2(x)}\right)\right], \tag{6}$$

with

$$R_0(x) = \frac{1}{\mathrm{GeV}}\left(\frac{x}{x_0}\right)^{\lambda/2}. \tag{7}$$

This dipole cross section exhibits colour transparency at small dipole radii r (i.e. $\hat{\sigma} \sim r^2$ for $r < R_0$) and saturation at large r (i.e. $\hat{\sigma} \sim \sigma_0$ for $r > R_0$). Saturation at low x is explicitly built-in through the x-dependent radius R_0.

After a fit to the inclusive structure function, the diffractive structure function follows as a prediction of this ansatz.

One interesting property of this model is the prediction that the ratio of diffractive to inclusive cross sections is roughly constant as a function of W, as has been observed experimentally [9].

Semi-classical model

In the semi-classical approach [19], an approximation is used in which the hadronic target is much larger than the transverse separation of the dipoles. Assuming further that the colour fields in distant parts of the target are uncorrelated, the relevant colour field configurations can be averaged, yielding explicit formulae for both the diffractive and inclusive parton distributions at some low scale Q_0^2. Diffraction occurs if the emerging partonic state is a colour singlet. A conventional DGLAP analysis is then used to calculate the diffractive and inclusive structure functions at larger values of Q^2. The model has four free parameters in total, which are obtained from a fit to the experimental data.

It is interesting to note that also in this model the diffractive gluon density turns out to be much larger than the diffractive quark density.

Two-gluon exchange model

This QCD calculation describes the diffractive $\gamma^* p$ interaction in terms of partonic fluctuations of the photon ($q\overline{q}$, $q\overline{q}g$, etc.) that scatter elastically off the proton through the exchange of two gluons in a net colour-singlet configuration [20]. An essential feature of the model is that the cross section is proportional to the square of gluon density inside the proton. The calculation requires high transverse momentum of all outgoing partons, thus making it particularly suited for diffractive high E_T jet production. In order to avoid the valence quark region in the proton and to exclude secondary reggeon exchanges, the range of validity is restricted to $x_{I\!P} < 0.01$.

4 Experimental results

In the following, Monte Carlo models are used to compare the measured hadron level cross sections to the predictions of the phenomenological models and QCD calculations presented in the previous section. RAPGAP [21] is used to obtain the predictions of the partonic pomeron model with different pomeron intercept values and parton distributions. The programme also contains implementations of the saturation and the semi-classical models as well as the two-gluon exchange model. Both versions of the soft colour interaction model are implemented in the LEPTO generator [22].

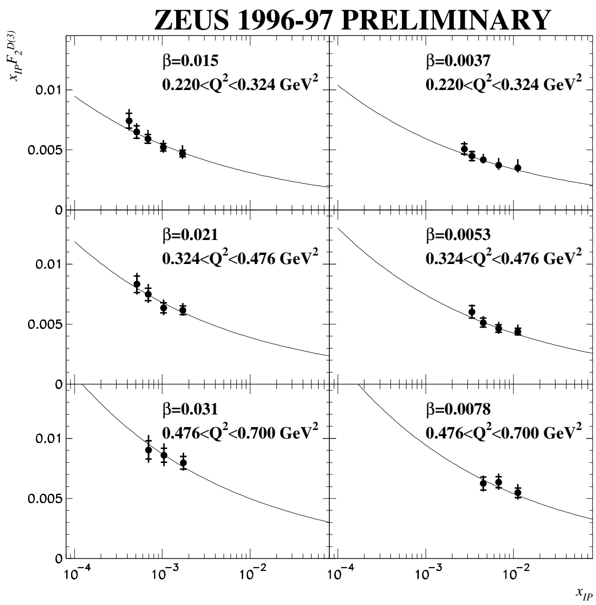

Fig. 2: The diffractive structure function $F_2^{D(3)}$ (multiplied by $x_{I\!P}$) is plotted as a function of $x_{I\!P}$ and shown in different bins of Q^2 (and β). The curves are the result of a simple Regge fit to the data (see text).

$0.22 < Q^2 < 0.70$ GeV^2
$90 < W < 220$ GeV
$3 < M_X < 12$ GeV
$M_Y < 6$ GeV

Table 1 Kinematic domain of the diffractive structure function measurement by ZEUS.

Inclusive cross section at low Q^2

New measurements of the inclusive diffraction cross section at very low Q^2 extend previous results at higher Q^2 into the transition region between photoproduction and deep inelastic scattering. This allows the evolution of the pomeron trajectory with Q^2 to be studied from the soft to the hard limit. Moreover, these new data provide a test of the saturation model which explicitly attempts to describe the behaviour of the inclusive and diffraction cross section at low Q^2 and low x.

Using their "Beam Pipe Calorimeter" (BPC) the ZEUS Collaboration obtained pre-

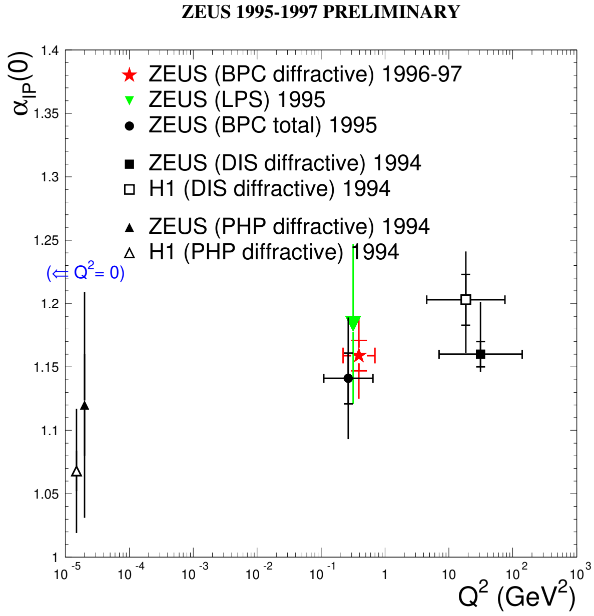

Fig. 3: Different measurements of the inclusive and diffractive structure function, obtained by H1 and ZEUS [7, 8, 23], are used to obtain the dependence of the pomeron intercept $\alpha_{I\!P}(0)$ as a function of the photon virtuality Q^2.

liminary cross sections for inclusive diffraction at low Q^2 based on 6.2 pb^{-1}. Diffraction events were selected with the "M_X subtraction method" [8] and restricted to the kinematic region listed in Tab. 1.

Figure 2 shows the diffractive structure function as a function of $x_{I\!P}$ in different bins of Q^2. Applying a simple Regge form $x_{I\!P}F_2^{D(3)} \propto 1/x_{I\!P}^{2\overline{\alpha}_{I\!P}-2}$ (with $\overline{\alpha}_{I\!P} = \alpha_{I\!P}(0) + \alpha'_{I\!P}\overline{t}$) to fit the data, results in an estimate of $\alpha_{I\!P}(0) = 1.159 \pm 0.012^{+0.027}_{-0.032}$ (assuming $\alpha'_{I\!P} = 0.25$ GeV^{-2} and $|\overline{t}| = 1/7.5$ GeV^2). This result is shown in Fig. 3 together with other estimates of $\alpha_{I\!P}(0)$ obtained from fits to published and preliminary data from H1 and ZEUS. Although the errors bars still remain large, the data (H1 data in particular) tend to show a rise of the diffractive $\alpha_{I\!P}(0)$ with Q^2.

A cross check of the ZEUS data using the "Leading Proton Spectrometer" (LPS) in roughly the same kinematic region yields an estimate of the proton dissociation background in the above data sample equal to $30 \pm 20\%$.

In order to explicitly study the saturation model, Fig. 4 shows the diffractive structure function as a function Q^2 in different bins of M_X and W. The diffractive structure function shows a similar behaviour to that of the inclusive structure function, rising linearly at low values of Q^2 and flattening off at higher Q^2. Provided that $q\overline{q}g$ are allowed

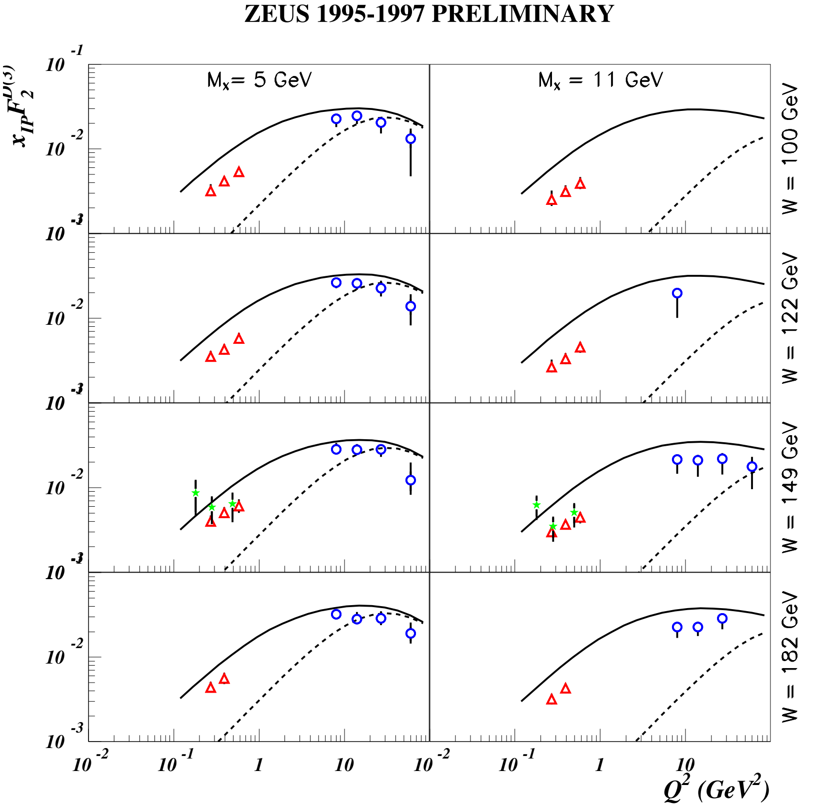

Fig. 4: The diffractive structure function (multiplied by $x_{I\!P}$) is plotted as a function of Q^2 in different bins of M_X and W and compared to predictions from the saturation model. Both the $q\overline{q}$ and the $q\overline{q}+q\overline{q}g$ contributions to the saturation model are shown. Data points labeled by $\triangle$ (ZEUS BPC preliminary) or $\circ$ (ZEUS 1994) were obtained with the M_X subtraction method and are scaled to remove the proton-dissociation background. The data points labeled with $\star$ (ZEUS LPS preliminary) were obtained with the "Leading Proton Spectrometer".

to contribute (especially at high M_X), the saturation model reproduces the shape of the low Q^2 transition region.

Diffractive high E_T jet production

The production of jets with large transverse energy provides an ideal test of the underlying dynamics of diffraction models [24]. The interaction mechanism, which is dominated by boson-gluon fusion, is highly sensitive to the role of gluons and the large transverse

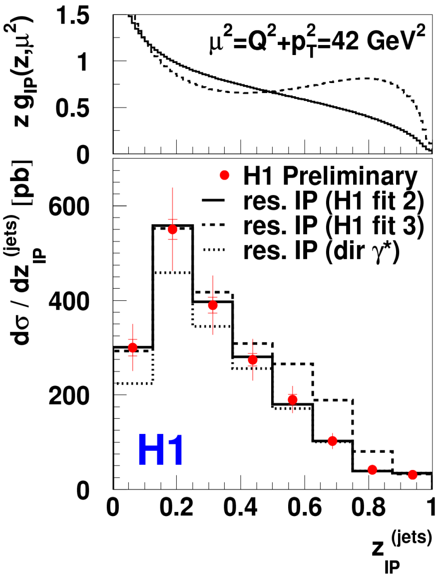

Fig. 5: The differential diffractive dijet cross section is displayed as a function of $z_{I\!P}^{jets}$ and compared with predictions from the partonic ("resolved") pomeron model. Different gluon density functions, obtained from fits to the inclusive cross section and shown in the top figure for an evolution scale which is typical for the dijet event sample, are used as input to the model. The effect of only including the direct photon contribution is also shown.

$4 < Q^2 < 80$ GeV^2
$0.1 < y < 0.7$
$x_{I\!P} < 0.05$
$M_Y < 1.6$ GeV
$\|t\| < 1$ GeV^2
$p_T^{jet} > 4$ GeV
$-3 < \eta^{jet} < 0$

Table 2 Kinematic domain of the diffractive dijet cross section measurement by H1.

energy lends a hard scale for perturbative calculations.

The H1 Collaboration recently obtained preliminary results based on an integrated luminosity of 17.9 pb^{-1}, resulting in approximately 2500 events with at least two jets in the final state system X. Diffractive events are selected by excluding any hadronic

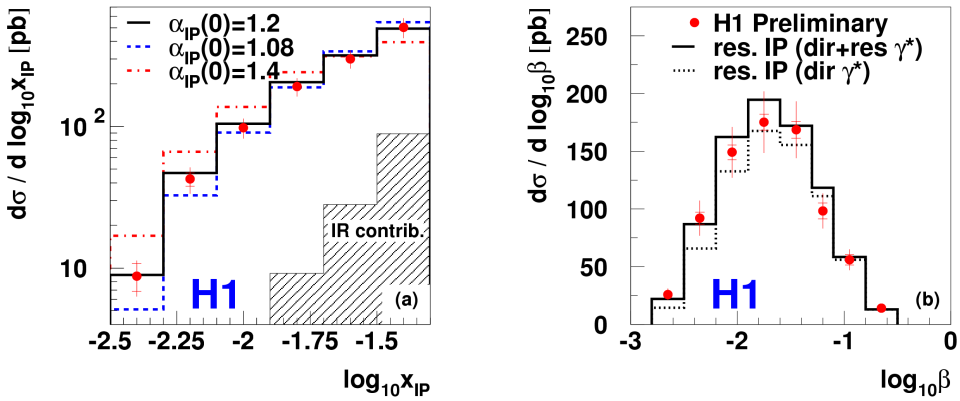

Fig. 6: The differential dijet cross section is displayed as a function of $x_{I\!P}$ (a) and β (b) and compared to the partonic pomeron model. Predictions are shown for different values of the pomeron intercept $\alpha_{I\!P}(0)$ and also the sub-leading reggeon component is displayed.

activity in the range $3.2 < \eta^{lab} < 7.5$ and jets are identified as collimated energy depositions in η-ϕ space within a cone of radius $R = \sqrt{\Delta\eta^2 + \Delta\phi^2} = 1$. The fraction of the pomeron momentum transferred to the dijet system, and therefore entering the hard scattering, can be calculated as follows:

$$z_{I\!P}^{jets} = \frac{Q^2 + M_{jj}^2}{Q^2 + M_X^2} \tag{8}$$

with M_{jj} the invariant mass of the dijet system. Differential cross sections are measured in the kinematic region defined in Tab. 2 as a function of many variables [25]. Here, only a selection of the available distributions is presented.

Figure 5 shows that applying the results of Regge-QCD fits, as obtained from the diffractive structure function [7], works very well. The analysis of the inclusive diffractive cross section yields two different fits with similar χ^2/ndf (cf. top of fig. 5), each with very similar quark densities but one with a flat gluon density function ("H1 fit 2") and another with a gluon density function that peaks at high values of the fractional momentum z ("H1 fit 3"). For the dijet cross section analysis it seems that the flat gluon distribution is slightly preferred over the peaked gluon density. Including the contribution of resolved photons further improves the agreement with the data, as can be expected, because for a large fraction of the dijet event sample the jet transverse momentum squared is actually larger than the virtuality of the photon ($p_T^2 > Q^2$).

The dijet event sample also provides an independent cross-check of the measurement of the pomeron intercept $\alpha_{I\!P}(0)$, as obtained from the Regge-QCD fits to the inclusive cross section. Figure 6 displays the $x_{I\!P}$ distribution whose slope is directly related to

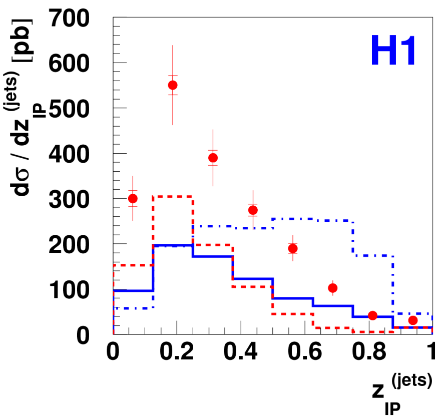

Fig. 7: The differential dijet cross section is displayed as a function of $z_{\mathbb{P}}$ and compared to different soft colour neutralisations models. The full and dashed-dotted (blue) lines represent the old and new (with general area law) soft colour interaction model; the dashed (red) line represents the semi-classical model.

$\alpha_{\mathbb{P}}(0)$. The dijet selection causes the distribution to rise instead of fall with increasing $x_{\mathbb{P}}$. The distribution is, however, still very sensitive to a change in the value of the pomeron intercept, as can be seen from the different Monte Carlo curves corresponding to a range in $\alpha_{\mathbb{P}}(0)$ between 1.08 and 1.4. Figure 6 also shows the contribution from secondary reggeon exchanges which is small and only visible at large $x_{\mathbb{P}}$. Note that the β distribution extends to much lower values than in the analysis of the inclusive cross section, where β-values down to 0.04 are reached.

Figure 7 compares the same experimental data to several soft colour neutralisation models. The original soft colour interaction model [15] and the semi-classical model [19] roughly agree and show the same trend as in the experimental data, although their normalisation is too low by a factor of two. The new soft colour interaction model (implementing the generalised area law) [16] has good normalisation, but the shape of the $z_{\mathbb{P}}$ distribution does not agree with the data.

Finally, Fig. 8 compares the $z_{\mathbb{P}}$ distribution obtained from data with the saturation model [18] and two-gluon exchange model [20]. Here an additional cut on $x_{\mathbb{P}}$ has been applied to avoid the valence quark region and to exclude sub-leading exchanges. The saturation model is somewhat low while the two-gluon exchange model roughly describes the data. As shown, the $q\overline{q}$ component of the two-gluon model is nearly negligible and the cross section is dominated by $q\overline{q}g$ partonic states. The two-gluon model requires a cutoff at low transverse momenta of the gluon in $q\overline{q}g$ states. Lowering this cutoff in p_T^2 to 0.5 GeV^2 significantly increases the cross section and affects mostly the low p_T pomeron remnant. The model is not able to describe data at $x_{\mathbb{P}} > 0.01$.

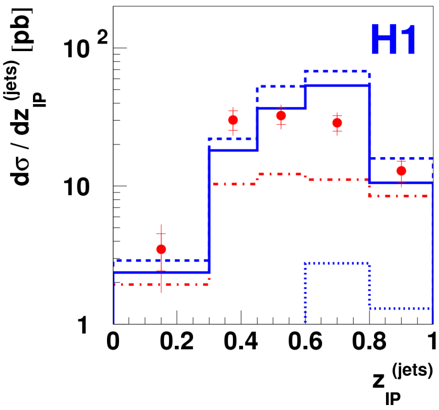

Fig. 8: The differential dijet cross section is displayed as a function of $z_{I\!P}$ and compared to the saturation and two-gluon models. The requirement $x_{I\!P} < 0.01$ has been applied in addition to the kinematic cuts of Tab. 2. The full, dashed and dotted lines are predictions from the two-gluon exchange model for the $q\bar{q}g$ component with a p_T^2 cutoff at 1 GeV^2, the $q\bar{q}g$ component with a p_T^2 cutoff at 0.5 GeV^2 and the $q\bar{q}$ component, respectively. The dashed-dotted line represents the saturation model.

$Q^2 > 5$ GeV^2
$200 < W < 250$ GeV
$x_{I\!P} < 0.025$
$M_X < 23$ GeV

Table 3 Kinematic domain of the diffractive 3-jet cross section measurement by ZEUS.

3-jet production in diffractive DIS

ZEUS obtained a preliminary measurement of the 3-jet cross section in diffractive DIS based on 39 pb^{-1}. In total some 5800 events with 3 jets in the final state were observed. Diffractive events were selected by exlcuding hadronic activity above $\eta_{max} = 3.0$ and restricted to the kinematic region listed in Tab. 3. Jets are found with a k_T clustering algorithm where a cut value $y_{cut} = 0.05$ is used because it gives the smallest hadronisation corrections according to Monte Carlo simulations.

For each jet a variable $x_i = 2E_i^{jet}/M_X$ is calculated and the jets are labelled such that $x_1 > x_2 > x_3$. Different values of x_i correspond to different topologies of the 3-jet final state as shown in Fig. 9. All possible configurations for a three-body final state are present in the data.

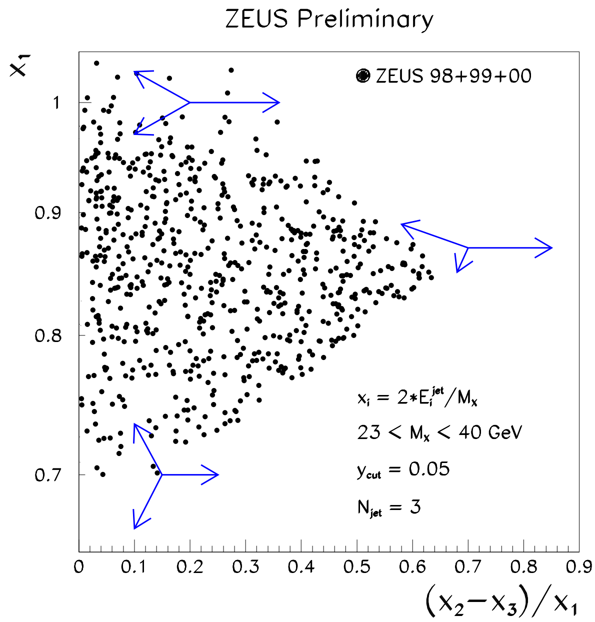

Fig. 9: 3-jet events are represented in a plane of x_1 vs. $(x_2 - x_3)/x_1$. Different regions in this plane correspond to different topologies of the three-body final state, as shown by the diagrams.

Projections of the 2-dimensional plot shown in Fig. 9 on the x_1 and $(x_2 - x_3)/x_1$ axes are shown in Fig. 10. When comparing the data to different models, it can be seen that the shape of the distributions is well reproduced by all models, but that the saturation and the 2-gluon exchange model have a normalization that is too low by about a factor of two. The partonic pomeron model is compatible with the data, given the quoted systematic errors and the uncertainty in the contribution from proton dissociation processes.

5 Summary

Recent preliminary results, obtained by the H1 and ZEUS collaborations, on the inclusive diffractive structure function at low Q^2 and on high E_T dijet and 3-jet production in diffractive deep inelastic scattering have been presented and compared to several theoretical models.

The cross section in the transition region between photoproduction and deep-inelas-

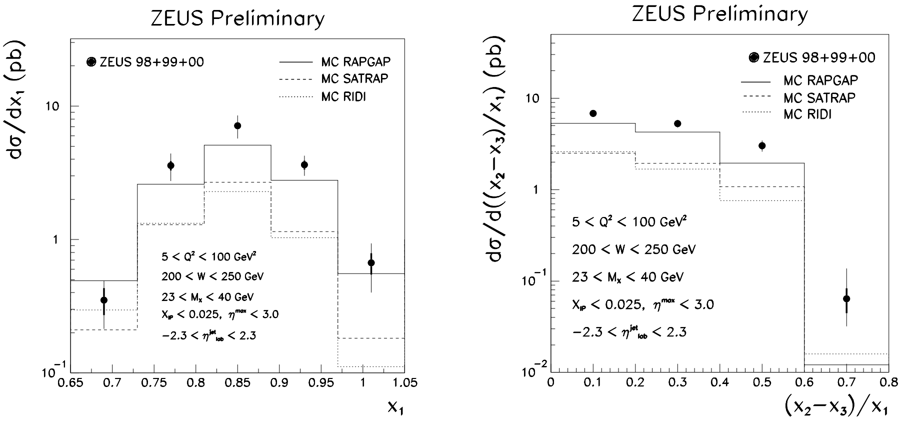

Fig. 10: Differential 3-jet cross sections are plotted as a function of x_1 amd $(x_2 - x_3)/x_1$ and compared to predictions from the partonic pomeron model (RAPGAP), the saturation model (SATRAP) and the 2-gluon exchange model (RIDI).

tic scattering is well reproduced by the saturation model using a combination of $q\overline{q}$ and $q\overline{q}g$ partonic states. Some tendency is observed for a rise of the pomeron intercept with Q^2 in the region from $Q^2 = 0$ to $Q^2 \approx 10$ GeV^2.

The partonic pomeron model, with a flat gluon density function ("H1 fit 2"), produces a very good description of all experimental data on jet production. The dijet analysis in particular thus confirms the picture of a hard pomeron ($\alpha_{I\!P}(0) = 1.2$) dominated by gluons carrying large fractional momenta.

The soft colour interaction, semi-classical and saturation models are either wrong in normalisation or in shape. As some of these models might be improved by including next-to-leading order contributions, it is presently not yet possible to make any final judgements on their validity.

Full perturbative QCD calculations, based on the exchange of two gluons in a colour-singlet configuration, are able to describe the differential dijet cross sections, but are limited to a kinematic domain where $x_{I\!P} < 0.01$.

Theoretical models are, however, rapidly evolving and with the large data samples that are expected to be collected after the HERA upgrade it will be possible to further discriminate between models.

Acknowledgement. I would like to thank the organizers of *Hadron Structure 2000* for their hospitality and the invitation to this interesting summer school-seminar. I appreciate the hard work of all members of the H1 and ZEUS collaborations who contributed to these results by collecting and analysing the experimental data.

References

[1] P. D. B. Collins, *Introduction to Regge Theory and High Energy Physics,* Cambridge University Press (1977).

[2] A. Donnachie and P. V. Landshoff, *Phys. Lett.* **B296** (1992) 227–232.

[3] J. R. Forshaw and D. A. Ross, *Quantum Chromodynamics and the Pomeron,* Cambridge University Press (1997).

[4] ZEUS Collaboration, M. Derrick et al., *Phys. Lett.* **B315** (1993) 481–493, *ibid.* **B346** (1995) 399–414;
H1 Collaboration, T. Ahmed et al., *Nucl. Phys.* **B429** (1994) 477–502, *ibid.* **B435** (1995) 3–22.

[5] G. Ingelman and P. Schlein *Phys. Lett.* **B152** (1985) 256.

[6] H1 Collaboration, T. Ahmed et al., *Phys. Lett.* **B348** (1995) 681–696;
ZEUS Collaboration, M. Derrick et al., *Z. Phys.* **C68** (1995) 569–584, J. Breitweg et al., *Eur. Phys. J.* **C1** (1998) 81–96.

[7] H1 Collaboration, C. Adloff et al., *Z. Phys.* **C76** (1997) 613–629.

[8] ZEUS CollaborationM. Derrick et al., *Z. Phys.* **C70** (1996) 391–412.

[9] ZEUS Collaboration, J. Breitweg et al., *Eur. Phys. J.* **C6** (1999) 43–66.

[10] ZEUS Collaboration, M. Derrick et al., *Phys. Lett.* **B338** (1994) 483–496, *Z. Phys.* **C67** (1995) 227–238, J. Breitweg et al., *Phys. Lett.* **B421** (1998) 368–384;
H1 Collaboration, S. Aid et al., *Z. Phys.* **C70** (1996) 609–620, C. Adloff et al., *Phys. Lett.* **B428** (1998) 206–220, *Eur. Phys. J.* **C1** (1998) 495–507, *ibid.* **C5** (1998) 439–452.

[11] V. N. Gribov and I. Ya. Pomeranchuk, Sov. Phys. JETP **15** (1962) 788L.

[12] J. C. Collins, *Phys. Rev.* **D57** (1998) 3051–3056, *ibid.* **D61** (2000) 019902 (erratum).

[13] L. Trentadue and G. Veneziano, *Phys. Lett.* **B323** (1994) 201–211;
A. Berera and D. E. Soper, *Phys. Rev.* **D53** (1996) 6162–6179.

[14] V. N. Gribov and L. N. Lipatov, Sov. J. Nucl. Phys. **15** (1972) 438–450 and 675–684;
Yu. L. Dokshitzer, Sov. Phys. JETP **46** (1977) 641–653;
G. Altarelli and G. Parisi, *Nucl. Phys.* **B126** (1977) 298.

[15] A. Edin, G. Ingelman and J. Rathsman, *Phys. Lett.* **B366** (1996) 371–378, *Z. Phys.* **C75** (1997) 57–70.

[16] J. Rathsman, *Phys. Lett.* **B452** (1999) 364–371.

[17] J. Bartels, J. Ellis, H. Kowalski and M. Wüsthoff, *Eur. Phys. J.* **C7** (1999) 443–458.

[18] K. Golec-Biernat and M. Wüsthoff, *Phys. Rev.* **D59** (1999) 014017.

[19] W. Buchmüller, M. F. McDermott and A. Hebecker, *Nucl. Phys.* **B487** (1997) 283–310;
W. Buchmüller, T. Gehrmann and A. Hebecker, *Nucl. Phys.* **B537** (1999) 477–500;.

[20] J. Bartels, H. Lotter and M. Wüsthoff, *Phys. Lett.* **B379** (1996) 239–248;
J. Bartels, C. Ewerz, H. Lotter and M. Wüsthoff, *Phys. Lett.* **B386** (1996) 389–396;
J. Bartels, H. Jung and M. Wüsthoff, *Eur. Phys. J.* **C11** (1999) 111–125.

[21] H. Jung, Comp. Phys. Comm. **86** (1995) 147–161.

[22] A. Edin, G. Ingelman and J. Rathsman, Comp. Phys. Comm. **101** (1997) 108–134.

[23] H1 Collaboration, C. Adloff et al., *Z. Phys.* **C74** (1997) 221;
ZEUS Collaboration, J. Breitweg et al., *Z. Phys.* **C75** (1997) 421–435.

[24] W. Buchmüller, M. F. McDermott and A. Hebecker, *Phys. Lett.* **B410** (1997) 304–310.

[25] F.-P. Schilling, Ph. D. thesis, University of Heidelberg, to be published.